Microfluidic Biochip for Impedance Spectroscopy of Biological Species

R. Gómez and R. Bashir*
School of Electrical and Computer Engineering
E-mail: bashir@ecn.purdue.edu

A. Sarikaya and M.R. Ladisch*
Department of Agricultural and Biological Engineering

J. Sturgis and J.P. Robinson*
Department of Basic Medical Sciences

T. Geng and A.K. Bhunia
Department of Food Science

H.L. Apple and S. Wereley
School of Mechanical Engineering, Purdue University, West Lafayette, IN 47907-1285

Abstract. This paper describes the fabrication and characterization of a microelectronic device for the electrical interrogation and impedance spectroscopy of biological species. Key features of the device include an all top-side processing for the formation of fluidic channels, planar fluidic interface ports, integrated metal electrodes for impedance measurements, and a glass cover sealing the non-planar topography of the chip using spin-on-glass as an intermediate bonding layer. The total fluidic path volume in the device is on the order of 30 nl. Flow fields in the closed chip were mapped by particle image velocimetry. Electrical impedance measurements of suspensions of the live microorganism *Listeria innocua* injected into the chip demonstrate an easy method for detecting the viability of a few bacterial cells. By-products of the bacterial metabolism modify the ionic strength of a low conductivity suspension medium, significantly altering its electrical characteristics.

Key Words. biochip, microfluidic, impedance, *Listeria*

1. Introduction

In recent years, there has been a merger of microelectronics and biological sciences to develop what are called ''biochips'' (Vo-Dinh and Cullum, 2000; Warsinke et al., 2000). The term biochip has been used in various contexts but can be defined as ''microfabricated devices that are used for processing (delivery, processing, and analysis) of biological species (molecules, cells, etc.).'' Such devices have been used, among other things, for the direct interrogation of the electric properties and behavior of cells (Borkholder et al., 1996; Ehret et al., 1997; Ayliffe et al., 1999); impedance-based detection of protein binding to surfaces, antigen-antibody binding, and DNA hybridization (DeSilva et al., 1995; Mirsky et al., 1997; Berggren et al., 1998; Van Gerwen et al., 1998a); micro-scale capillary electrophoresis (Woolley and Mathies, 1995; Harrison et al., 1996); and optical detection of DNA hybridization using fluorescence signals in the commercially available ''DNA-chips'' (Fodor et al., 1991; Heller, 1996).

One of the most interesting uses of biochips is for the detection of small quantities of pathogenic bacteria or toxigenic substances in food, bodily fluids, tissue samples, soil, etc. In applications such as the screening of food products for the presence of pathogenic bacteria, the goal is to detect between 100 and 1000 microorganisms per milliliter of sample, with a sample volume of a couple of milliliters. Not counting the fact that bacteria are substantially larger than single biomolecules ($\sim 2\,\mu m$ vs. ~ 10–$100\,\text{Å}$), 1000 cells are approximately equivalent to a 10^{-5} femto-moles of cells, which gives an idea of the difficulty in directly detecting such a small amount suspended in a volume of 1 or 2 ml, along with large numbers of food debris, proteins, carbohydrates, oils, and other bacteria. Additionally, in many cases the screening technique must be able to discern between viable and dead cells. Many bacteria will not produce toxins when not viable and consequently will not be pathogenic in that state. DNA detection methods, which search for DNA sequences specific to the pathogen of interest (Wang et al., 1997), can be extremely sensitive because

---

they rely on the very specific binding of complementary DNA strands, often coupled with polymerase chain reaction (PCR) for amplification. But the detected DNA fragments cannot reveal whether the pathogen was viable or not. These are the main reasons current methods of detection almost always involve a growth step, in which the bacteria are cultured to increase their numbers by several orders of magnitude. Once the bacteria are amplified to a large number, visual detection of colonies or enzyme-linked immunosorbent assays (ELISA) confirm their presence in the original sample. Even though bacteria can multiply very rapidly, this amplification by means of extended growth makes conventional detection methods extremely lengthy, taking anywhere from two to seven days. Thus, one of the main goals of micro-scale detection is a reduced time of analysis, on the order of 2 to 4 hours, to be better than the more conventional methods like plate counts and ELISA.

Numerous reports can be found in the literature on biosensors based on the impedimetric detection of biological binding events (DeSilva et al., 1995; Mirsky et al., 1997; Berggren et al., 1998; Van Gerwen et al. 1998a), or the amperometric detection of enzymatic reactions (Hoshi et al., 1994; Jobst et al., 1997; Towe and Pizziconi, 1997). Impedimetric detection works by measuring impedance changes produced by the binding of target molecules to receptors (antibodies, for example) immobilized on the surface of microelectrodes. Amperometric devices measure the current generated by electrochemical reactions at the surface of micro-electrodes, which are commonly coated with enzymes. Both of these methods can be very sensitive, but preparation of the surfaces of the electrodes (immobilization of antibodies or enzymes) is a complex and sometimes unreliable process, they can be prone to drift (Riepl et al., 1999), and tend to be very sensitive to noise produced by the multitude of species present in real samples (bodily fluids, food, soil, etc.).

Most of the above-mentioned devices are not fully integrated biochips, and sometimes lack integrated electrodes and a sealed fluidic path for the injection and extraction of samples. The most common design of these sensors uses thin metal rods or wires as electrodes, immersed in a flow-through cell (Hoshi et al., 1994; Towe and Pizziconi, 1997; Berggren et al., 1998; Mirsky et al., 1998). And even those devices based on microfabricated biochips either have a fluidic system separately fabricated over the chip (DeSilva et al., 1995; Schöning et al., 1998), or the samples are dropped over an open reservoir on the chip (Paeschke et al., 1996; Berney et al., 1997; Van Gerwen et al., 1998b), or the whole chip is immersed in a vessel containing the fluids. Having a fully closed system permits the incorporation of sample pre-processing

steps, like filtering and chromatography, onto the same chip as the detector.

As mentioned earlier, one of the main goals of bacterial sensors is to determine whether the bacterium of interest is indeed live or dead. A technique that has been widely reported to detect the viability of bacteria on a macro-scale relies on measuring the conductance/impedance changes of a medium in which the microbes are cultured (Felice et al., 1999; Wawerla et al., 1999; Edmiston and Russell, 2000). Such a method is recognized by the Association of Official Analytical Chemists International (AOAC) as a standard technique for the detection of *Salmonella* in food (Gibson et al., 1992; AOAC, 1996). This is possible because bacterial metabolism changes the electrolyte concentration in the suspension medium, significantly altering its electrical characteristics.

This paper presents the construction details of a microfabricated biochip with integrated fluidic paths and electrodes which will be used to perform micro-scale electronic measurements of biological solutions. The device will also be used to investigate whether a change in conductance in nanoliter volumes of bacterial suspensions can be measured and used to indicate the viability of the bacteria. Device fabrication is presented and fluid flow through the chip is demonstrated using 2 μm fluorescently-labeled beads imaged through a fluorescence microscope. Preliminary electrical impedance measurements are also presented to demonstrate that the device can be used to distinguish between different concentrations of the bacterium *Listeria innocua*, a non-pathogenic strain of *Listeria*, by the change in conductance of the suspension produced by bacterial metabolism. These concentrations represent very few bacterial cells in the very small volumes (nanoliters) of the measurement chambers of the biochip.

2. Fabrication

2.1. *Channels and electrodes*

The device features an all top-side processing to form wells and channels on a silicon wafer. A silicon wafer is used to allow the future integration of other electronic detectors or active electronic circuitry in later versions of the chip. The entire fabrication process is depicted in Figure 1 and proceeds as follows: Silicon wafers with a thickness of 450 μm and (1 0 0) orientation are oxidized to have a 0.45 μm thick SiO_2 layer, and a series of rectangular cavities, connected by channels, are etched into the oxide (Figure 1a). Potassium hydroxide (KOH) is used to etch the silicon surface to a depth of about 12 μm using the thermally-grown SiO_2 as a hard mask. This depth is still within the depth of focus of the mask aligner
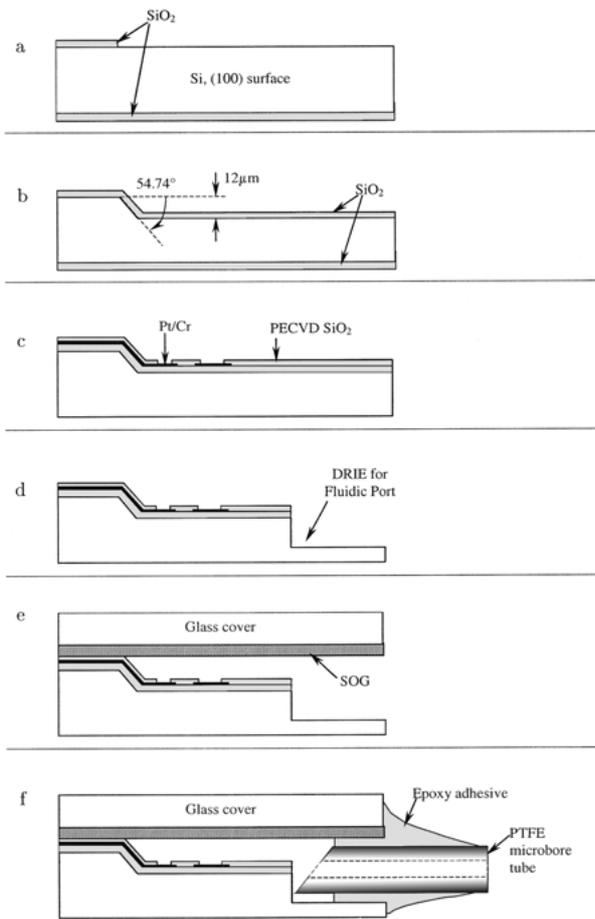
Fig. 1. *Steps in the fabrication process of the biochip: (a) Definition of a SiO₂ hard mask for etching the channels. (b) Anisotropic etching of the channels followed by re-oxidation. (c) Deposition and patterning of metal electrodes, followed by SiO₂ deposition for insulation. (d) Deep Reactive Ion Etch (DRIE) of fluidic port trenches. (e) Bonding of the glass cover. (f) Bonding of microbore tubes into the fluidic ports.*

used, thus guaranteeing a good definition of patterns at the bottom of the etched areas. Since the surface of the wafer is a (100) plane, the etched channels and cavities have tapered walls forming an angle of 54.74° with respect to the surface of the wafer (Figure 1b). Such an angle permits the deposition of metal over the walls, allowing for metal traces to run into and across the channels without breaks. After the KOH etching, the SiO₂ hard mask is completely removed and the wafer is oxidized at 1050°C for 60 minutes in wet-O_2 to form a 0.45 μm thick layer of SiO₂. Electrodes at the bottom of the cavities, and metal traces connecting them to the bonding pads on the periphery of the die are defined over the oxide by lift-off, using a 5 μm thick photoresist layer (AZ4620 from Clariant Corp., New Jersey, U.S.A.). The photoresist layer needs to be thick enough to keep it from cracking at the upper edges of the channel walls due to the tension that builds up during baking (Duey, 1988).

The metallization is formed by RF-sputtering of an 800 Å thick layer of platinum over a 600 Å thick film of chromium, the latter serving as an adhesion layer. The sheet resistance of the metallization is approximately 30 Ω·cm (2.1 Ω/square for the given thickness). After the metal is deposited and patterned, a 0.6 μm thick SiO₂ film is deposited by plasma-enhanced chemical vapor deposition (PECVD) to insulate the electrodes and metal traces. This film is subsequently wet-etched to open windows over the electrodes at the bottom of the cavities and over the bond and probe pads (Figure 1c). These windows leave only the top platinum surface exposed, which is fairly resistant to chemical attack, while keeping the chromium covered so that it does not interact with, or is not affected by any of the solutions that may flow through the channels. Figure 2 shows an electron micrograph of a section of the device, where electrodes are defined at the bottom of wells, and metal lines cross the channels.

2.2. Coverglass bonding

The channels are hermetically sealed by bonding a rectangular piece of glass, 0.17 to 0.25 mm thick (No. 2
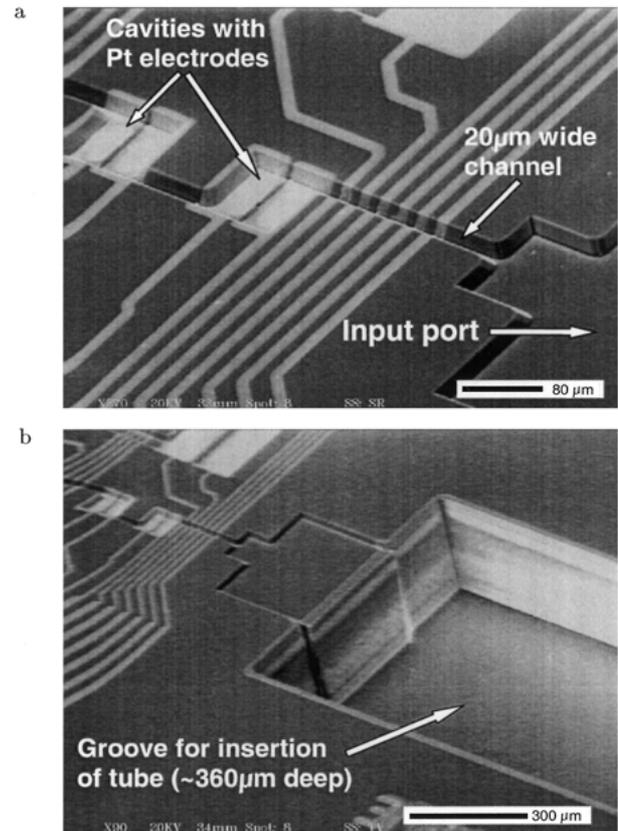

Fig. 2. *Scanning electron micrograph of (a) the biochip channels with integrated electrodes, and (b) fluid I/O port created using deep reactive ion etch.*

Dow Corning microscopy glass covers), to the surface of the chip. Initially, attempts were made to anodically bond the glass cover but the results were very poor for what we believe are two main reasons: (1) The oxide layer on the silicon wafer is very thick (almost $1\,\mu m$), which decreases the magnitude of the electric field that is established between the silicon substrate and the glass cover, and thus decreases the bonding force between them. (2) Additionally, the bulges created on the surface of the die by the platinum traces, connecting the electrodes in the channels to the bond pads on the periphery of the die, were too close to each other ($10\,\mu m$) preventing the glass from deforming to fill the space between them. These open grooves in between the platinum traces prevented the formation of a tight seal.

A much better bond is achieved by using a low-melting-temperature Spin-On-Glass (SOG) as adhesive (Dragoi et al., 1999) (Figure 1e). This SOG is a methylsilsesquioxane polymer (Methylsilsesquioxane 400F from Filmtronics Inc., Pennsylvania, U.S.A.) that flows at temperatures between 150°C and 210°C (Spin-On-Glass, 1998). The flowing SOG fills the grooves in between the platinum traces and any other surface irregularities, providing a perfectly hermetic seal, while the low flow temperature minimizes thermally-induced stresses and damage to temperature-sensitive materials on the die. The glass cover is first cut to the desired size in a diamond saw, thoroughly rinsed in DI water, dried, and cleaned in Ar/O_2 plasma for 20 minutes. After cleaning, the SOG is spun on the glass at 5000 r.p.m. for 40 seconds and dried in a convection oven at 90°C for 2 minutes. This process results in a SOG film approximately $3000\,\mathring{A}$ thick according to the data-sheet provided by the manufacturer (Spin-On-Glass, 1998). The glass is then manually aligned onto the die (SOG side down) and clamped in place. Subsequently, the clamped assembly is heated on a hot plate to 100°C for 5 minutes, followed by 180°C for 5 minutes, and 200°C for at least 1 hour to cure the SOG film. Although the manufacturer indicates that the SOG must be cured at 400°C for 30 minutes (Spin-On-Glass, 1998), extensive cracking of the SOG film was observed if the bonded assembly was exposed to temperatures above 300°C. Most likely, the cause of this cracking is the large mismatch between the thermal expansion coefficients of the die, the glass cover, and the SOG. For this reason, to minimize the stress in the SOG film the curing temperature is kept at 200°C, which seems to be sufficient for a reliable bond. The curing time could be substantially increased to compensate for the lower temperature, but even a one hour cure produces a bond capable of withstanding the maximum pressures that have been applied to drive fluids through the microchannels ($\sim 340\,$kPa at an external sample reservoir). A single pressurization test of one fully functional device, with no flow, indicated a failure pressure of approximately $700\,$kPa. At this pressure the glass started to unbind from the chip and leaks appeared in the region around the input/output ports.

2.3. *Fluidic ports*

One of the challenges that exists in the development of microfluidic biochips is creating reliable fluidic interfaces to the macro-world. For the design of the biochip described, connections for injecting samples into the device are created by etching deep trenches running up to the edge of the die, into which microbore tubes can be inserted horizontally as depicted in Figure 1f. This configuration has several advantages over the standard top connection through the sealing cover. The length of the trenches can be adjusted to provide a large bonding surface which improves the robustness and reliability of the connection; in this case the trenches were made 2 mm long and $700\,\mu m$ wide. Locating the tubes horizontally results in a planar structure that is easier to package and handle. And there is no need for fine alignment between the channels on the chip and the sealing cover, which would be necessary if the input/output ports were on the cover. The trenches are created by a deep reactive ion etch (DRIE) system (Plasma Therm SLR770 system using the Bosch Etch process), to a depth of approximately $390\,\mu m$, with a $10\,\mu m$ photoresist layer as mask (Figure 1d). The etch-rate is about $1.6\,\mu m/$min. with a selectivity to photoresist of approximately $75:1$. A protrusion at the edge between the shallow trench and the deep trench (see Figure 2b) appears because the photoresist hardmask flows during the bake step prior to the DRIE.

The tubes are bonded into the trenches after the glass cover is attached to the device. Before bonding, the tip of the tubes is treated with FluoroEtch (Acton Technologies Inc., Pennsylvania, U.S.A.) to improve its bondability (by forming a carbonaceous layer on the surface), and it is cut at an angle to keep the bore from being blocked by the trench wall. The tubes are inserted into the trenches and the remaining void in the trenches is filled with biomedical grade epoxy adhesive (Durabond M-121HP from Loctite Corp., Connecticut, U.S.A.), which penetrates into the trench by capillarity (Figure 1 f). Even very rough handling of the tubes does not compromise the integrity of the bond.

3.   *Flow Characterization*

After fabrication, particle imaging velocimetry (PIV) was used to demonstrate and study the flow through the microchannels. PIV indirectly measures the flow velocity using tracer particles that are homogeneously suspended
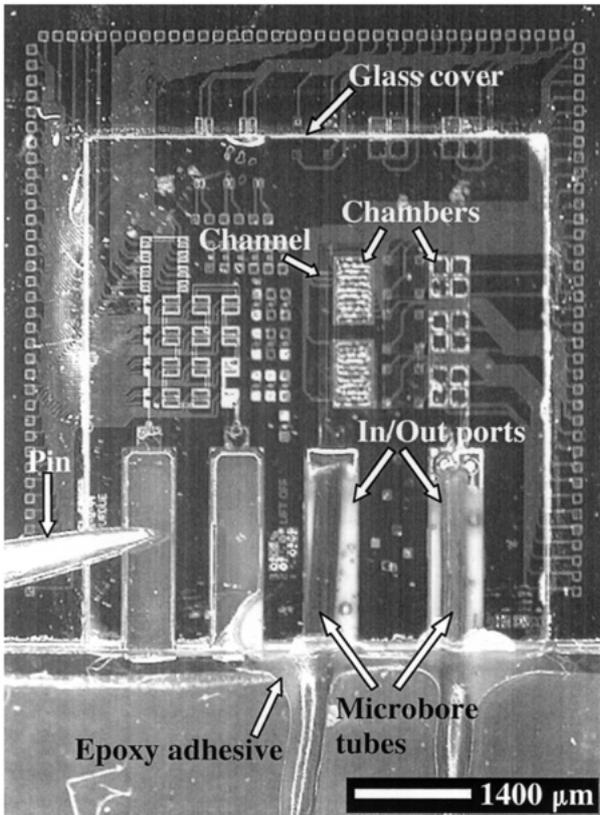
in the liquid. By following the trajectories of the particles over time, the velocimetry system can determine the velocity field of the liquid at a grid of measurement points distributed throughout the whole channel (Meinhart et al., 1999). In this particular experiment, water-based suspensions of fluorescein-labeled latex beads (Sigma-Aldrich, St. Louis, Missouri, U.S.A.), with a mean diameter of 1.88 μm, at concentrations between 10^7 and 10^8 particles/ml, were injected into the microchannels and imaged at $20 \times$ magnification with an epi-fluorescence microscope (Nikon Labophot, Nikon Inc., Melville, New York, U.S.A.) outfitted with a high sensitivity CCD camera (Optronics 470T, Optronics, Goleta, California, U.S.A.). A constant intensity mercury lamp was used to illuminate the flow, while the images were recorded in real-time at video rate (30 Hz) either directly on a computer, or on standard VHS video equipment and digitized later. PIV software, especially optimized for microscopic flows, was used to analyze the digital images of the flow tracers and produce vector maps of the velocity field. This software is described at length elsewhere (Wereley and Meinhart, 2000). Figure 4 shows the velocity field in a rectangular well in the microchip. For pressures up to 20.7 kPa, fluid velocities
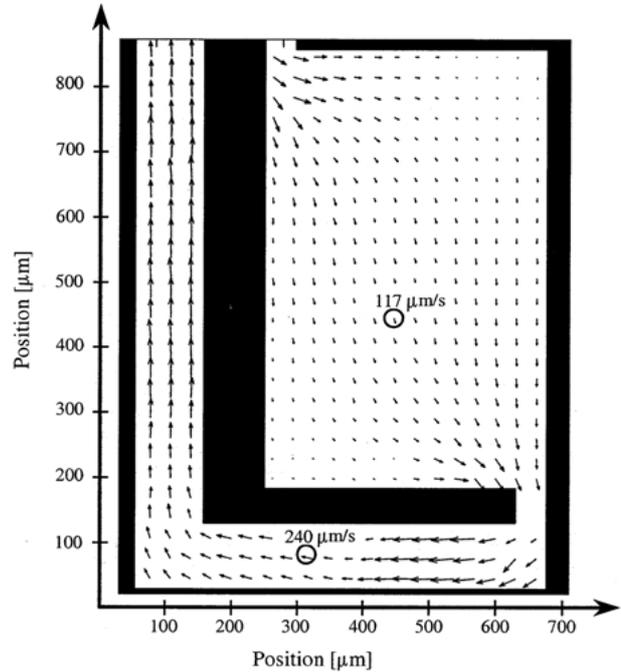

Fig. 4. *Fluid velocity field in a section of the channels, obtained using particle velocimetry.*

in the channels range from about 100 μm/s to 1600 μm/s depending on the region of the wells where velocity is measured and the specific pressure applied to drive the flow. A parameter widely used to characterize the regime in which flow ocurrs is the Reynolds number, defined as (Fox and McDonald, 1998):

$$\mathrm{Re} = \frac{\rho v D_h}{\mu}, \tag{1}$$

where ρ, v, and μ are the density, velocity, and viscosity of the fluid, respectively. D_h is the hydraulic diameter, defined as $4S/P$, where S and P are the channel cross-sectional area (perpendicular to the flow direction) and perimeter, respectively. The Reynolds number represents the ratio of inertial to viscuous forces and determines whether the flow will be laminar or turbulent. A Reynolds number much smaller than unity indicates that the flow is laminar, without recirculating areas (dead zones), while around and above unity vortices can appear. In our experiments, the measured velocities give a Reynolds number on the order of 10^{-3} to 10^{-2} (i.e., viscuous foces dominate the flow), resulting in perfectly laminar, creeping flow, without any recirculating or stagnant areas. Recirculating or stagnant regions should be avoided because transport of solvated or suspended species into and out of those regions occurs exclusively by diffusion, which is a very slow process and would severely affect the performance of any sensing elements placed there. Recirculation and stagnation will also cause

cross-contamination of samples injected into the chip because any substances in these areas cannot be rapidly flushed out.

4. Impedance of Bacterial Suspensions

As was mentioned earlier, there are several reports in the literature dealing with the detection of pathogenic bacteria in food by monitoring the conductance or the impedance of a specially formulated culture medium innoculated with extracts from food samples (Felice et al., 1999; Wawerla et al., 1999; Edmiston and Russell, 2000). This is possible because bacterial metabolism changes the electrolyte concentration in the suspension medium, significantly altering its electrical characteristics. Most of these conductivity measurements are performed with DC signals, yielding no information about interfacial phenomena at the solution-electrode interfaces. But Felice et al., (1999) claim that measuring some of the interfacial parameters using an AC excitation (at a single frequency, or preferably at multiple frequencies) makes the technique more sensitive.

A fairly simple circuit model of a pair of electrodes immersed in an electrolytic solution is shown in Figure 5 (Jacobs et al., 1998), where C_{di} is the dielectric capacitance (it contains contributions from all the materials surrounding the electrodes, including the solution), R_s is the bulk solution resistance (charge transport across the bulk), and Z_w is the interfacial impedance (the so-called Warburg impedance), which accounts for the changes in the electrolyte concentration gradient at the interface (Bard and Faulkner, 1980; Vetter, 1967). The simplest model of the interfacial response to AC signals, yields the following expression for Z_w:

$$Z_w = \frac{\sigma(1-j)}{\omega^{1/2}}, \tag{2}$$

where $j = \sqrt{-1}$, ω is the angular frequency of the electrical signal, and σ is a parameter that depends on the

diffusive properties of the electrolytes, and the area and characteristics of the electrodes. From this expression we can see that the phase difference between the applied voltage and the resulting current will be 45° at all frequencies. However, actual systems show that the phase difference can be anywhere between 0° and 90°, while still remaining constant over frequency. Thus, a better model for the interfacial impedance is (Jacobs et al., 1998):

$$Z_w = \frac{1}{(j\omega)^{nB}}, \tag{3}$$

where n and B are parameters that depend on the properties of the electrolytes and of the electrodes. Equation 3 assumes that the phase between voltage and current is constant at $n\pi/2$ rad.

Preliminary experiments to study the effects of bacterial metabolism on the electrical properties of the suspension medium were carried out using the described biochip. The main purpose of these experiments was to determine whether impedance measurements in the microscale could provide information about the metabolic activity of a small number of bacteria. Metabolic activity could then be used as an indicator of bacterial viability. Impedance measurements were done in a chamber that is 530 μm wide by 850 μm long by 12 μm deep, for a total volume of 5.27 nl (taking into account that the walls of the well have a 54.74° angle). This chamber has two interdigitated platinum electrodes with five fingers each. The exposed area of each finger is 450 μm by 50 μm, and the distance between finger centers is 80 μm. A HP4284A LCR meter (Hewlett Packard Corp., now Agilent Technologies, Palo Alto, California) measured the impedance of the interdigitated electrodes at 52 frequencies, logarithmically spaced between 100 Hz and 1 MHz, with a 50 mV (amplitude) voltage excitation. The impedance of the wiring and probes was automatically substracted from the measurements, so that only the impedance of the elements in the chip was recorded.

Listeria innocua was cultured in brain heart infusion (BHI) broth (Difco Laboratories, Detroit, Michigan) for 16 hours at 37°C, then washed four times by centrifugation and re-suspension in a low conductivity Tris-Glycine (Tris-Gly) buffer to eliminate all the electrolytes present in the culture broth. Tris-Gly buffer contains 0.18 mM Tris, ~ 47 mM Glycine, plus 0.05% (vol/vol) Tween-20 (a detergent). This detergent is necessary to prevent sticking of the cells to each other and to the chip, which would clog the microscopic channels in the biochip. The nominal pH and conductivity of the buffer are 7.5 and 33.5 μS/cm, respectively. The Tris concentration was modified
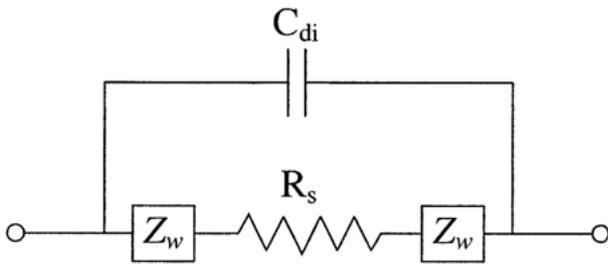

Fig. 5. *Equivalent circuit of a pair of electrodes immersed in and electrolyctic solution ($C_d i$ = Dielectric capacitance, R_s = Bulk solution resistance, Z_w = Interfacial impedance).*

around the nominal value to adjust the pH close to 7.5. Previous (unpublished) macro-scale experiments using live and heat-killed *L. innocua* had clearly indicated that the bacteria remain alive in the Tris-Gly buffer and that their metabolism does indeed change the buffer conductance. After washing, the bacteria were re-suspended at concentrations of $\sim 10^5$, $\sim 10^7$, $\sim 10^8$, and $\sim 10^9$ cells/ml in Tris-Gly buffer. These concentrations result in approximately 0.53, 53, 530, and 5300 bacterial cells (in average) in the 5.27 nl chamber, respectively. Afterwards, dextrose was added to each suspension at a concentration of 2.2 mg/ml and the suspensions were incubated at 37°C for 2 hours to promote bacterial growth, along with a sample of buffer with dextrose, without bacteria, as control. Following incubation, the samples were refrigerated at 2°C until the measurements were performed. All samples were injected into the chip using pressurized nitrogen, and were allowed to flow through the chip for 15 minutes, before measuring, to properly flush the whole fluidic path.

Figure 6 shows the complex impedance (magnitude and angle) as a function of frequency for six different samples injected into the biochip: De-ionized (DI) water with a conductivity of 0.06 µS/cm, Tris-Gly buffer with 2.2 mg/ml dextrose, and the four *L. innocua* suspensions mentioned above. Figure 7 shows the difference between the measured complex impedance of Tris-Gly buffer and the impedance of each one of the *L. innocua* suspensions ($\Delta Z = Z_{\text{buffer}} - Z_{\text{bacteria}}$). For frequencies between 2 kHz and 20 kHz most of the difference in impedance from buffer to each one of the suspensions is due to changes in the resistive components, as evidenced by a phase close to 0° for ΔZ in this frequency range. The circuit model

Fig. 7. *Difference between the complex impedance of Tris-Gly buffer and each one of the* L. innocua *suspensions ($\Delta Z = Z_{\text{buffer}} - Z_{\text{bacteria}}$).*

shown in Figure 5 was fitted to the measured curves, with Z_w given by equation 3, and an additional series resistor R_{tr} that accounts for the resistance of the metal traces on the biochip, connecting the bonding pads to the electrodes in the chamber. Values of $R_{tr} = 2889\,\Omega$ and $C_{di} = 17.98$ pF were extracted from fitting to the Tris-Gly buffer data and held fixed when fitting the model to all other samples. Figure 8 shows an example of how well the chosen model fits the measured impedances. The values of R_s, n, and B obtained from the fits to all the samples are contained in Table 1. Having n close to 1.0 for all samples, with the exception of DI water, indicates that the interface is mostly capacitive, with a small parallel resisitve component. Figure 9 compares the following normalized differences for the various cell concentrations:
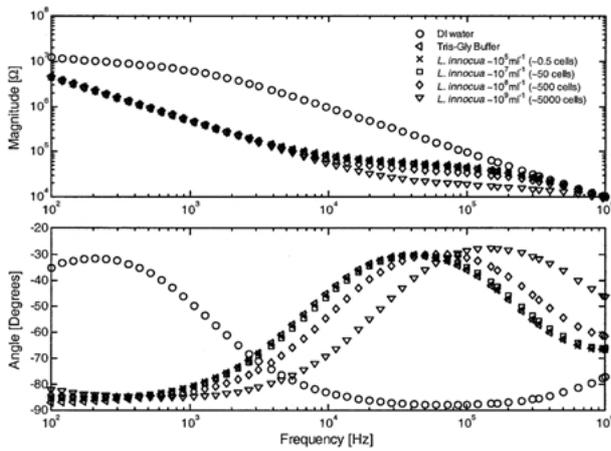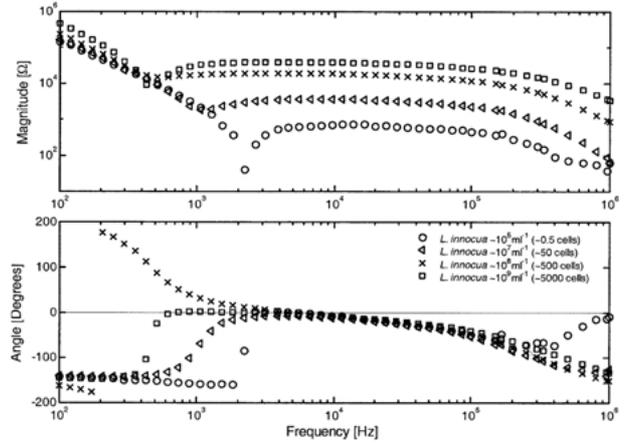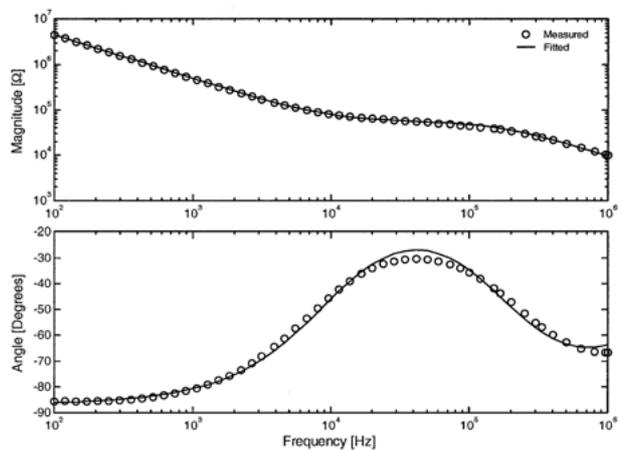
Fig. 6. *Measured complex impedance (magnitude and angle) of the different samples injected into the biochip. The numbers of cells in the legend correspond to the numbers present in the chamber where the measurement was performed (V = 5.27 nl).*

Fig. 8. *Fit of the circuit model in Figure 5 to the measured complex impedance of the* L. innocua *suspension at a concentration of $\sim 10^5$ cells/ml.*
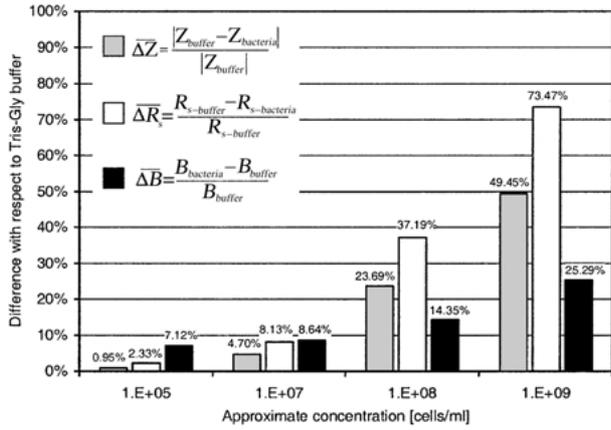
Fig. 9. *Normalized differences* $\overline{\Delta Z}$, $\overline{\Delta R_s}$ *amd* $\overline{\Delta B}$, *for each concentration of* L. innocua, *as defined in equation 4.*

$$\overline{\Delta Z} = \frac{|Z_{\text{buffer}} - Z_{\text{bacteria}}|}{|Z_{\text{buffer}}|}, \quad \text{at } f = 11.43 \text{ kHz} \qquad (4a)$$

$$\overline{\Delta R_s} = \frac{R_{s-\text{buffer}} - R_{s-\text{bacteria}}}{R_{s-\text{buffer}}} \qquad (4b)$$

$$\overline{\Delta B} = \frac{B_{\text{bacteria}} - B_{\text{buffer}}}{B_{\text{buffer}}}. \qquad (4c)$$

At the lowest concentration, the difference in B is larger than that in Z and R_s, while above 10^7 cells/ml R_s shows the largest differences with respect to buffer. Detection can rely on both $\overline{\Delta R_s}$ and $\overline{\Delta B}$ to increase the sensitivity at the lowest concentrations. These results indicate that if the small number of *Listeria* cells present in a food or soil sample can be captured and retained in a chamber in the biochip, their viability could be assesed by measuring the change in impedance of the electrodes in the chamber. Fewer than 10 cells in a 5.27 nl volume could in principle produce a change of $\sim 7\%$ in the parameter B, provided that any ionic contamination coming from the sample can be completely removed and that the chamber is filled with a low conductivity buffer (with appropriate nutrients to promote growth).

5. Conclusions

We have described the fabrication process for a microfluidic biochip that is used for impedance spectroscopy of biological species. Key features of the device include an all top-side processing for the formation of fluidic channels, planar fluidic interface ports, integrated metal electrodes for impedance measurements, and a glass cover sealing the non-planar topography of the chip using spin-on-glass as an intermediate bonding layer. The total volume of the fluidic path in the device is on the order of 30 nl. Flow fields in the closed chip were mapped by particle image velocimetry. Preliminary measurements of the AC impedance of *L. innocua* suspensions in a low conductivity buffer were performed using the biochip. Bacterial metabolic activity alters the electrolyte concentration of the buffer, and thus modifies its electrical characteristics. The response of a simple circuit model can be fitted to the measured impedance as a function of frequency, and the changes in the parameters of the model could be used as indicators of the metabolic activity of the bacteria. Very small numbers of viable bacterial cells (1 to 5000) injected in a 5.27 nl chamber in the biochip produce a sizeable difference in the impedace of a pair of electrodes placed in the chamber, with respect to the impedance produced by plain buffer (without bacteria). This difference could, in principle, be used to detect the viability of small numbers of bacterial cells extracted from food, soil, or bodily fluid samples, in a couple of hours

6. Acknowledgments

Table 1. *Parameters resulting from fitting the circuit model to the impedance data shown in Figure 6*

Sample	Number of cells in 5.27 nl	Bulk solution resistance R_s [kΩ]	n	$B[\times 10^{-12}]$
DI water	0	242.0	0.149	5.83×10^4
Tris-Gly Buffer	0	56.58	0.968	800.6
$\sim 10^5$ cells/ml	0.527	55.26	0.961	857.6
$\sim 10^7$ cells/ml	52.7	51.98	0.960	869.7
$\sim 10^8$ cells/ml	527	35.54	0.952	915.5
$\sim 10^9$ cells/ml	5270	15.01	0.945	1003.1

References

AOAC, *Official methods of analysis of AOAC International,* 16th ed. (Association of Official Analytical Chemists International, Gaithersburg, MD, 1996).

H. Ayliffe, A. Frazier, and R. Rabbitt, IEEE Journal of Microelectromechanics **8**(1), 50–57 (1999).

A.J. Bard and L.R. Faulkner, *Electrochemical Methods* (John Wiley & Sons, 1980).

C. Berggren, B. Bjarnason, and G. Johansson, Biosensors and Bioelectronics **13**, 1061–1068 (1998).

H. Berncy, J. Alderman, W. Lane, and J. Collins, Sensors and Actuators B **44**, 578–584 (1997).

D. Borkholder, I. Opris, N. Maluf, and G. Kovacs, Annual International Conference of the IEEE Engineering in Medicine and Biology—Proceedings, 106–107, IEEE. (1996).

M. DeSilva, Y. Zhang, P. Hesketh, G. Maclay, S. Gendel, and J. Stetter, Biosensors and Bioelectronics **10**, 675–682 (1995).

V. Dragoi, M. Alexe, M. Reiche, and U. Gösele, CAS'99 Proceedings, 1999 International Semiconductor Conference, **2**, 443–446 (IEEE, 1999).

S. Duey, Master's thesis, Purdue University (1988).

A. Edmiston and S. Russell, Journal of Food Protection **63**(2), 264–267 (2000).

R. Ehret, W.B.M.B.A.S.K. Stegbauer, and B. Wolf, Biosensors and Bioelectronics **12**(1), 29–41 (1997).

C. Felice, R. Madrid, J. Olivera, V. Rotger, and M. Valentinuzzi, Journal of Microbiological Methods **35**, 37–42 (1999).

S. Fodor, M. Read, J. Pirrung, L. Stryer, A. Lu, and D. Solas, Science **251**, 767–773 (1991).

R. Fox and A. McDonald, *Introduction to Fluid Mechanics* (John Wiley & Sons, 1998).

D. Gibson, P. Coombs, and D. Pimbley, Journal of AOAC International **75**(2), 293–302 (1992).

F. Harrison, K. Fluri, N. Chiem, T. Tang, and Z. Fang, Micromachining, Sensors and Actuators B **33**, 105–109 (1996).

M. Heller, IEEE Engineering in Medicine and Biology **15**, 100–103 (1996).

T. Hoshi, J. Anzai, and T. Osa, Analytica Chimica Acta **289**, 321–327 (1994).

P. Jacobs, W. Hofer, R. Rossau, A.V. de Voorde, P.V. Gerwen, and P. Detemple, Proceedings of the Second International Conference on Microreaction Technology (New Orleans, LA, U.S.A., 223–229, 1998).

G. Jobst, I. Moser, P. Svasek, M. Varahram, Z. Trajanoski, P. Wach, P. Kotanko, F. Skrabal, and G. Urban, Sensors and Actuators B **43**, 121–125 (1997).

C. Meinhart, S. Wereley, and J. Santiago, Experiments in Fluids **27**(5), 414–419 (1999).

V. Mirsky, M. Mass, C. Krause, and O. Wolfbeis, Analytical Chemistry **70**, 3674–3678 (1998).

V. Mirsky, M. Riepl, and O. Wolfbeis, Biosensors and Bioelectronics **12**(9–10), 977–989 (1997).

M. Paeschke, L. Buchman, R. Seitz, and R. Hintsche, *Microsystem Technologies 96*, 687–692 (VDE-Verlag GMBH, 1996).

M. Riepl, V. Mirsky, I. Novotny, V. Tvarozek, V. Rehacek, and O. Wolfbeis, Analytica Chimica Acta **392**, 77–84 (1999).

M. Schöning, M. Thust, M. Müller-Veggian, P. Kordoš, and H. Lüth, Sensors and Actuators B **47**, 225–230 (1998).

Spin-On-Glass, *Methylsilsesquioxane 400F Product Data Sheet* (Filmtronics Inc., Pennsylvania, U.S.A., 1998).

B.C. Towe and V.B. Pizziconi, Biosensors and Bioelectronics **97**(9), 893–899 (1997).

P. Van Gerwen, W. Laureyn, W. Laureys, G. Huyberechts, M. Op De Beeck, K. Baert, J. Suls, W. Sansen, P. Jacobs, L. Hermans, and R. Mertens, Sensors and Actuators B **49**, 73–80 (1998a).

P. Van Gerwen, A. Varla, G. Huyberechts, M. Op De Beeck, K. Baert, W. Sansen, L. Hermans, and R. Mertens, *Microreaction Technology: Proceedings of the First International Conference on Microreaction Technology* 289–293 (Springer-Verlag, 1998b).

K.J. Vetter, *Electrochemical Kinetics* (Academic Press, 1967).

T. Vo-Dinh and B. Cullum, Fresenius Journal of Analytical Chemistry **366**, 540–551 (2000).

J. Wang, G. Rivas, C. Parrado, X. Cai, and M. Flair, Talanta **44**, 2003–2010 (1997).

A. Warsinke, A. Benkert, and F. Scheller, Fresenius Journal of Analytical Chemistry **366**, 622–634 (2000).

M. Wawerla, A. Stolle, B. Schalch, and H. Eisgruber, Journal of Food Protection **62**(12), 1488–1496 (1999).

S. Wereley and C. Meinhart, Proceedings of the 10th International Symposium on the Application of Laser Techniques to Fluid Mechanics (2000).

A. Woolley and R. Mathies, Analytical Chemistry **67**(20), 3676–3680 (1995).